Int. J. Electrochem. Sci., 8 **(2013)** 4346 - 4360

International Journal of
ELECTROCHEMICAL
SCIENCE
www.electrochemsci.org

Investigation of the Inhibitive Effect of 2-(Ethylthio)-1,4,5-Triphenyl-1*H*-Imidazole on Corrosion of Steel in 1 M HCl

L. Afia[1]*, N. Rezki*[2]*, M. R. Aouad*[2]*, A. Zarrouk*[3]*, H. Zarrok*[4]*, R. Salghi*[1*,5]*, B. Hammouti*[3,5] *,*
M. Messali[2]*, S. S. Al-Deyab*[5]

[1]Equipe de Génie de l'Environnement et de Biotechnologie, ENSA, Université Ibn Zohr, BP 1136, Agadir, Morocco.
[2]Chemistry Department, Faculty of Science, Taibah University, 30002, Al-Madinah AlMounawara, Saudi Arabia
[3]LCAE-URAC18, Faculté des Sciences, Université Mohammed Premier, Oujda, Morocco.
[4]Laboratory of the Separation Processes, University Ibn Tofail, Faculty of the Sciences, P.O. Box 1246 Kénitra Morocco.
[5]Petrochemical Research Chair, Chemistry Department, College of Science, King Saud University, P.O. Box 2455, Riyadh 11451, Saudi Arabia.
[*]E-mail: r_salghi@yahoo.fr

Received: 12 January 2013 / *Accepted:* 15 February 2013 / *Published:* 1 March 2013

The influence of 2-(ethyllthio)-1,4,5-triphenyl-1H-imidazole(DNSO) on the corrosion of mild steel in 1M HCl solution has been studied by weight loss measurements, potentiodynamic polarizations and electrochemical impedance spectroscopy (EIS). The inhibiting action increases with the concentration of the tested inhibitor. The highest efficiency 91% is obtained at 3.10^{-3} of DNSO. We note good agreement between gravimetric and electrochemical methods (potentiodynamic polarisation and EIS). Data, obtained from EIS measurements, were analyzed to model the corrosion inhibition process through appropriate equivalent circuit model; a constant phase element (CPE) has been used. Polarization measurements show also that DNSO act as good mixed inhibitor. DNSO is adsorbed on the steel surface according to a Langmuir isotherm adsorption model.

Keywords: Corrosion. Steel. Inhibition. DNSO. Acid medium.

1. INTRODUCTION

Mild steel is always exposed to the action of acid in industrial processes where acids play important roles such as in oil well acidizing, acid pickling, acid cleaning and acid descaling. The use of inhibitors is one of the best methods of protecting metals against corrosion [1,2]. The synthesis of new organic molecules offers various molecular structures containing several heteroatoms and substituents.

Many researches on inhibitors have been carried out, especially on nitrogen-containing inhibitor, the effect of these compounds on the corrosion behaviour of iron and steel in acidic solutions has been well documented [3-9]. These Organic compounds rich in heteroatoms such sulphur, nitrogen and oxygen generally exhibit the best protection among corrosion. Their adsorption is generally explained by the formation of an adsorptive film of a physical and/or chemical character on the metal surface. The modes of adsorption depend mainly on the chemical structure of the inhibitor, the chemical composition of the solution, the nature of the metal surface and the electrochemical potential of the metal–solution interface. Adsorption of inhibitors may blocks either cathodic, anodic, or both reactions. Data in the literature show that most organic inhibitors adsorb on metals by displacing water molecules on the surface and forming a compact barrier film [10-12].

Research in these latest decennia has permitted to classify several series containing S atom such aminoacid and aminoester [13-17], azole [18-24] and pyridine [25-28] as effective corrosion inhibitors.

In the present work, inhibitive action of DNSO on corrosion behaviour of C38 steel in 1M HCl has been studied by gravimetric method and electrochemical techniques such as potentiodynamic polarization and electrochemical impedance spectroscopy (EIS). The structural formula of the inhibitor examined is given in Fig. 1.

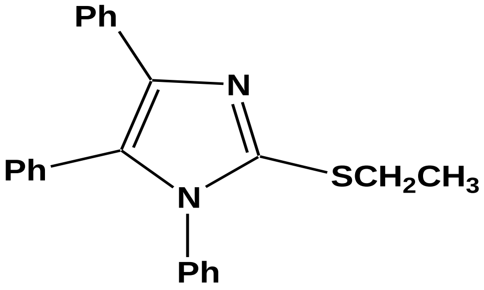

2

Figure 1. Structure of the investigated compound.

2. EXPERIMENTAL METHODS

2.1.Measurements and equipments

The new synthesized compound was characterized by ^{1}H NMR and FTIR spectroscopies. ^{1}H NMR (400 MHz) spectra were obtained in DMSO at room temperature. Chemical shifts (d) were reported in ppm to a scale calibrated for tetramethylsilane (TMS), which is used as an internal standard. The microwave-assisted reactions were performed using a controllable single-mode microwave reactor, CEM Discovery, designed for synthetic use. The reactor is equipped with a magnetic stirrer as well as a pressure, temperature and power controls. The maximum operating pressure of the reactor is 20 bar. The power and temperature range are 15 - 300 W and 60 – 250 ºC, respectively.

Conventional versus Microwave assisted synthesis of 2-ethylthio-1,4,5-triphenylimidazole (2)

This formal work describes the synthesis of new 2-ethylthio-1,4,5-triphenylimidazole (2) by the alkylation of 1,4,5-triphenylimidazole-2-thiol (**1**) with ethyl iodide, under both conventional and MW irradiation. Thus, the alkylation in presence of triethylamine in ethanol for 2 hours afforded the corresponding thioethyl imidazole **2** in 91%; subjection to MW irradiation required 2 min to afford 97% yield (Scheme 1).

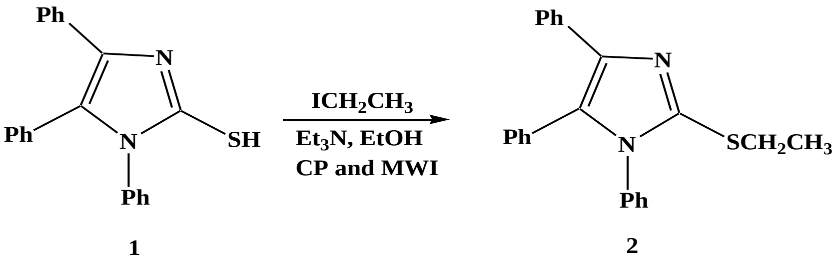

Scheme 1

Conventional procedure (CP). To a mixture of 1 (10 mmol) and triethylamine (11 mmol) in ethanol (50 mL), ethyl iodide (11 mmol) was added. The mixture was heated under reflux for 1 h. The ethanol was removed under reduced pressure and the product was recrystallized from ethanol. Yield 91%.

Microwave irradiation (MWI). A mixture of 1 (1 mmol), triethylamine (1.1 mol), ethanol (5 mL) and ethyl iodide (1.1 mmol) in a closed vessel was irradiated by MW for 2 min. The obtained mixture was treated as described above. Yield 97%. ; IR (KBr): 1538 (C=C), 1630 (C=N) cm^{-1}. ^{1}H NMR ($CDCl_3$): δ 1.15 (t, 3H, CH_2CH_3), 236-2.41 (q, 2H, CH_2CH_3), 7.20-7.48 (m, 15H, Ar-H).

2.2. Weight loss measurements

Coupons were cut into 2 × 2 × 0.08 cm^3 dimensions having composition (0.179% C, 0.165% Si, 0.439% Mn, 0.203% Cu, 0.034% S and Fe balance) are used for weight loss measurements. Prior to all measurements, the exposed area was mechanically abraded with 180, 320, 800 grades of emery papers. The specimens are washed thoroughly with bidistilled water, degreased and dried with ethanol. Gravimetric measurements are carried out in a double walled glass cell equipped with a thermostated cooling condenser. The solution volume is 80 cm^3. The immersion time for the weight loss is 8 h at 298 K.

2.3. Electrochemical tests

The electrochemical study was carried out using a potentiostat PGZ100 piloted by Voltamaster software. This potentiostat is connected to a cell with three electrode thermostats with double wall (Tacussel Standard CEC/TH). A saturated calomel electrode (SCE) and platinum electrode were used as reference and auxiliary electrodes, respectively. The material used for constructing the working electrode was the same used for gravimetric measurements. The surface area exposed to the electrolyte is 0.056 cm^2. Potentiodynamic polarization curves were plotted at a polarization scan rate of 0.5 mV/s. Before all experiments, the potential was stabilized at free potential during 30 min. The polarisation curves are obtained from −800 mV to −400 mV at 298 K. The solution test is there after de-aerated by bubbling nitrogen. Gas bubbling is maintained prior and through the experiments. In order to investigate the effects of temperature and immersion time on the inhibitor performance, some test were carried out in a temperature range 298–328 K. The electrochemical impedance spectroscopy (EIS) measurements are carried out with the electrochemical system (Tacussel), which included a digital potentiostat model Voltalab PGZ100 computer at E_{corr} after immersion in solution without bubbling. After the determination of steady-state current at a corrosion potential, sine wave voltage (10 mV) peak to peak, at frequencies between 100 kHz and 10 mHz are superimposed on the rest potential. Computer programs automatically controlled the measurements performed at rest potentials after 0.5 hour of exposure at 298 K. The impedance diagrams are given in the Nyquist representation. Experiments are repeated three times to ensure the reproducibility.

2.4. Solutions preparation

The aggressive solution (1M HCl) was prepared by dilution of analytical grade 37% HCl with double distilled water. The solution tests are freshly prepared before each experiment.

3.RESULTS AND DISCUSSION

3.1. Effect of concentration

3.1.1.Polarization curves

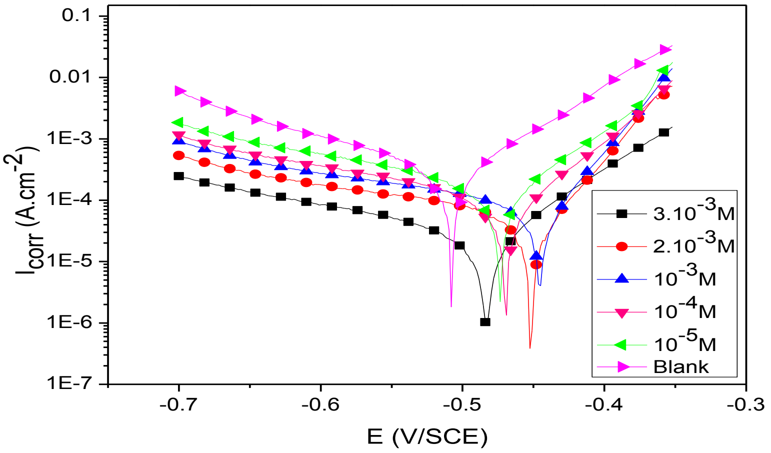

Figure 2. Potentiodynamic polarisation curves of C38 steel in 1M HCl in the presence of different concentrations of DNSO.

Potentiodynamic polarisation curves of C38 steel in 1M HCl in the absence and presence of DNSO at different concentrations at 298 K are presented in Fig. 2. The corrosion parameters including corrosion current densities (I_{corr}), corrosion potential (E_{corr}), cathodic Tafel slope (bc), anodic Tafel slop (ba) and inhibition efficiency (EI %) are listed in Table 1.

Table 1. Electrochemical parameters of C38 steel at various concentrations of DNSO in 1M HCl and corresponding inhibition efficiency.

Conc (M)	E_{corr} (mV/SCE)	I_{corr} (µA/cm^2)	-b_c (mV/dec)	b_a (mV/dec)	E_I (%)
Blank	-508	301	-150	69	-
1×10^{-5}	-473	155	-103	38	38.3
1×10^{-4}	-469	105	-154	46	60.6
1×10^{-3}	-445	84	-196	31	69.1
2×10^{-3}	-452	56	-149	31	79.8
3×10^{-3}	-541	27	-180	55	90.4

In this case, the inhibition efficiency is defined as follows:

$$E\% = (1 - \frac{I'_{corr}}{I_{corr}})x100 \qquad (1)$$

Where I_{corr} and I'_{corr} are current density in absence and presence of DNSO, respectively. We noted that I_{corr} and I'_{corr} was calculated from the intersection of cathodic and anodic Tafel lines.

Inspection of the Fig.2 reveals that the polarization curves are shifted toward more negative potentials and less current density upon addition of DNSO. This result confirms the inhibitive action of the DNSO toward acid corrosion of steel [31]. Addition of DNSO affects both anodic dissolution of steel and cathodic reduction reactions indicating that the two compounds could be classified as mixed-type inhibitors. We also remark that the cathodic current-potential curves give rise to Tafel lines, which indicate that hydrogen evolution reaction is activation controlled. The cathodic Tafel slope values in the presence of APE are different of that in its absence; we may deduce that DNSO modifies the mechanism of the reduction process [32]. The inhibition efficiency reaches 90.4% at 3×10^{-3} M. Consequently, DNSO is a good inhibitor.

3.1.2. Electrochemical impedance spectroscopy measurements

Fig. 3 shows the Nyquist plots for C38 steel in 1 M HCl solution in the absence and presence of different concentrations of the DNSO at 298K. The obtained Nyquist impedance diagrams in most cases does not show perfect semicircle, generally attributed to the frequency dispersion as a result of roughness and inhomogenates of the electrode surface. The data reveal that, each impedance diagram consists of a large capacitive loop with low frequencies dispersion (inductive arc). The shape is maintained throughout the whole concentrations, indicating that almost no change in the corrosion mechanism occurred due to the inhibitor addition [33].

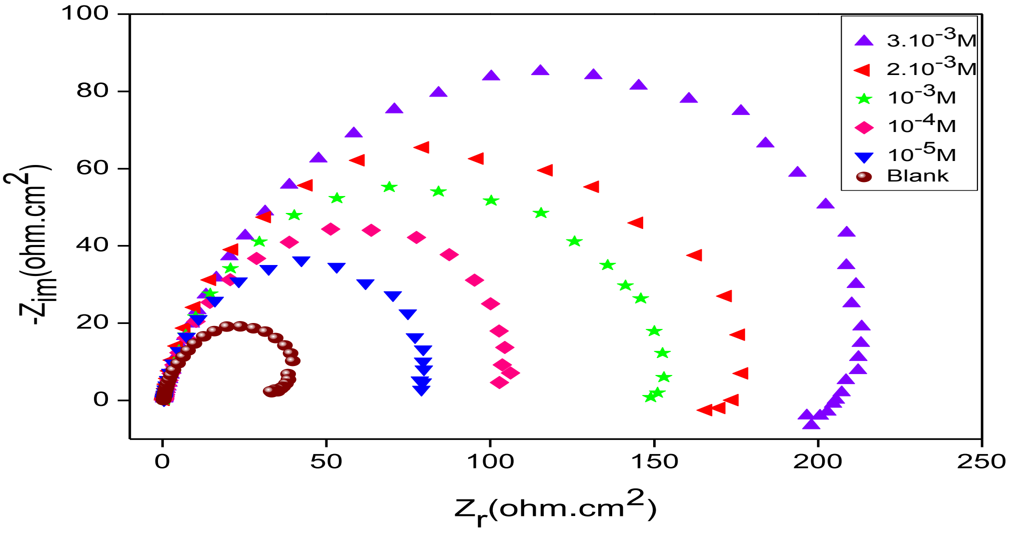

Figure 3. Nyquist diagrams for C38 steel electrode with and without DNSO at E_{corr}

The circuit consists of a constant phase element (CPE) Q, in parallel with a resistor R_t The use of CPE-type impedance has been extensively described in [34-35]:

$$Z_{CPE} = [Q(jw)^n]^{-1} \qquad (2)$$

The above equation provides information about the degree of non-ideality in capacitance behavior. Its value makes it possible to differentiate between the behavior of an ideal capacitor (n = 1) and of a CPE (n < 1). Considering that a CPE may be considered as a parallel combination of a pure capacitor and a resistor that is inversely proportional to the angular frequency, the value of capacitance, C_{dl}, can thus be calculated for a parallel circuit composed of a CPE (Q) and a resistor (R_t), according to the following formula [36-37]:

$$Q = (C_{dl}R_t)^n/R_t \qquad (3)$$

The impedance spectra with one capacitive loop were analyzed by using the circuit in Fig. 4 [38, 39], and the double layer capacitance (C_{dl}) was calculated in terms of Eq. 3.

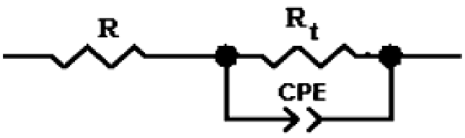

Figure 4. The equivalent circuit of the impedance spectra obtained for DNSO.

As an example, the Nyquist and Bode plot for DNSO at 10^{-4} M in 1M HCl are presented in Fig. 5a and b, respectively.

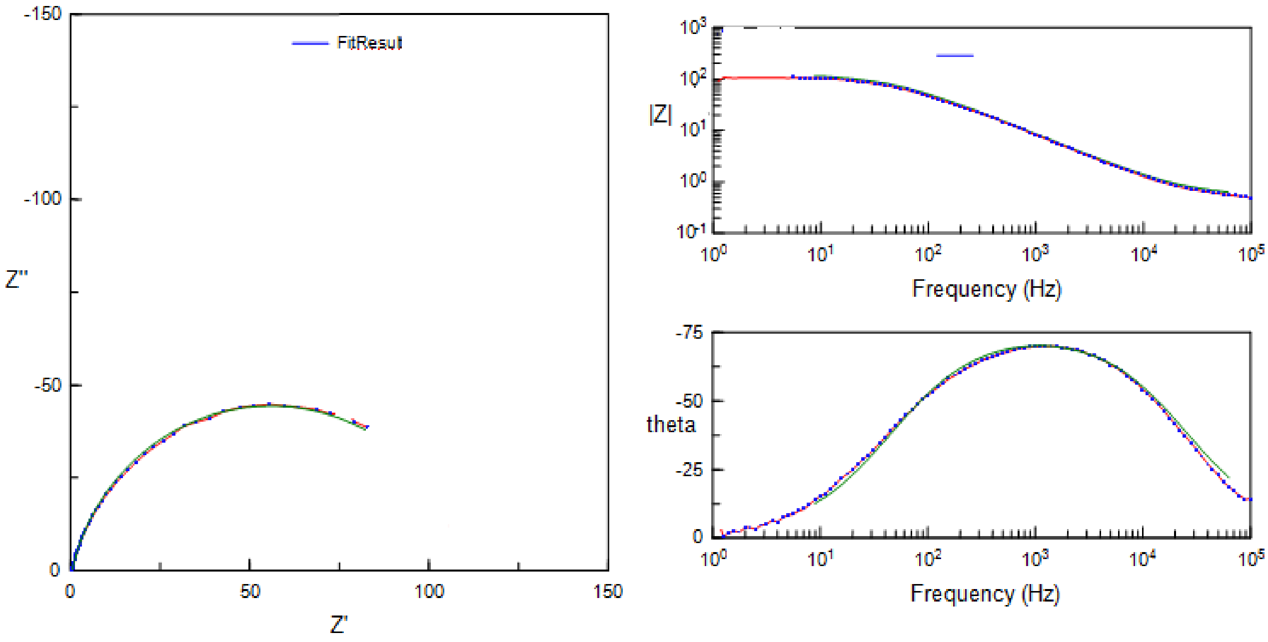

(a) **(b)**

Figure 5. EIS Nyquist (a) and Bode (b) plots for mild steel / 1M HCl + 10^{-4} of DNSO interface

Excellent fit with this model was obtained with our experimental data (Fig. 3). It is observed that the fitted data match the experimental, with an average error of about 0.01%. R_t values were simultaneously determined by analysis of the complex-plane impedance plots and the equivalent circuit model and the result are very similar with insignificant changes.

The inhibition efficiency can be calculated by the following formula:

$$E_{Rt}\% = \frac{(R_t - R^{\circ}{}_t)}{R_t} x100 \qquad (4)$$

Were R_t and $R^0{}_t$ are the charge transfer resistances in inhibited and uninhibited solutions respectively.

The electrochemical impedance parameters derived from these investigations are mentioned in Table 2.

Table 2. Electrochemical Impedance parameters for corrosion of steel in acid medium at various concentration of DNSO.

Conc (M)	R_t (Ω cm^2)	Q×10^{-3} ($s^n\ \Omega^{-1}cm^{-2}$)	C_{dl} (μF cm^{-2})	n	E_{RT} (%)
Blank	35.0	0.26370	77.0	0.8984	-
1×10^{-5}	74.6	0.15545	51.3	0.8922	53.1
1×10^{-4}	110.5	0.07026	36.8	0.8604	68.3
1×10^{-3}	132.0	0.05885	28.8	0.8680	73.5
2×10^{-3}	161.0	0.04946	20.1	0.8852	78.3
3×10^{-3}	223.0	0.01376	14.4	0.8259	84.3

The corresponding electrochemical parameters given in Table 2 reveal that introduction of DNSO into the acid corrodent caused the charge transfer resistance to increase, while reducing the double-layer capacitance. This effect becomes more pronounced at higher DNSO concentration. This increase in the diameter of the Nyquist semicircle (R_t values), including the corresponding increase in the magnitude of the phase angle peaks in inhibited solutions, points toward improved corrosion resistance due to the corrosion-inhibiting action of DNSO.

The decrease in C_{dl} values, which normally results from a decrease in the dielectric constant and/or an increase in the double-layer thickness, can be attributed to the adsorption of DNSO onto the metal/electrolyte interface. Efficiency of inhibition is observed from Table 2 to increase with DNSO concentration to reach 84.3% at 3 $\times10^{-3}$M. The results obtained from the polarization technique in acidic solution were in good agreement with those obtained from the electrochemical impedance spectroscopy (EIS) with a small variation.

3.1.3.Weight loss, corrosion rates and inhibition efficiency

The effect of the addition of DNSO tested at different concentrations on the corrosion of steel in 1M HCl solution was studied by using weight-loss at 298 K. Inhibition efficiency E_w (%) is calculated as follows:

$$E_W(\%) = \frac{W_{corr} - W'_{corr}}{W_{corr}} \times 100 \qquad (5)$$

Where W_{corr} and W'_{corr} are the corrosion rate of C38 steel in 1M HCl in absence and presence of inhibitor, respectively.

Table 3 regroups the results of weight loss of steel in 1M HCl with and without the addition of various concentrations of the DNSO.

From Table 3, it can be seen that corrosion rate values in 1.0 M HCl solution containing DNSO, decreased as the concentration of inhibitor increased. This result is due to fact that the adsorption amount and coverage of inhibitor on mild steel surface increases with inhibitor concentration. The highest inhibition efficiency of 90.6% was obtained at 3.10^{-3}M of DNSO.

Table 3. Effect of DNSO concentration on corrosion data of steel in 1M HCl.

W_{corr} (mg cm^{-2})	W'_{corr} (mg cm^{-2})	E_w (%)
Blank	1.8614	-
1×10^{-5}	0.9402	49.5
1×10^{-4}	0.5908	68.3
1×10^{-3}	0.4689	74.8
2×10^{-3}	0.3341	82.1
3×10^{-3}	0.1742	90.6

This result suggests that increase in inhibitor concentration increases the number of molecules adsorbed onto steel surface and reduces the surface area that is available for the direct acid attack on the metal surface. The results obtained from weight loss are in good agreement with electrochemical studies.

3.2. Effect of temperature

3.2.1. Polarization curves

Temperature has a great effect on the corrosion phenomenon. Generally the corrosion rate increases with the rise of the temperature. For this purpose, we made potentiostatic polarization in the range of temperature 298 to 328 K, in the absence and presence of DNSO at 10^{-3}M. The corresponding data are shown in fig 6,7 and Table 4.

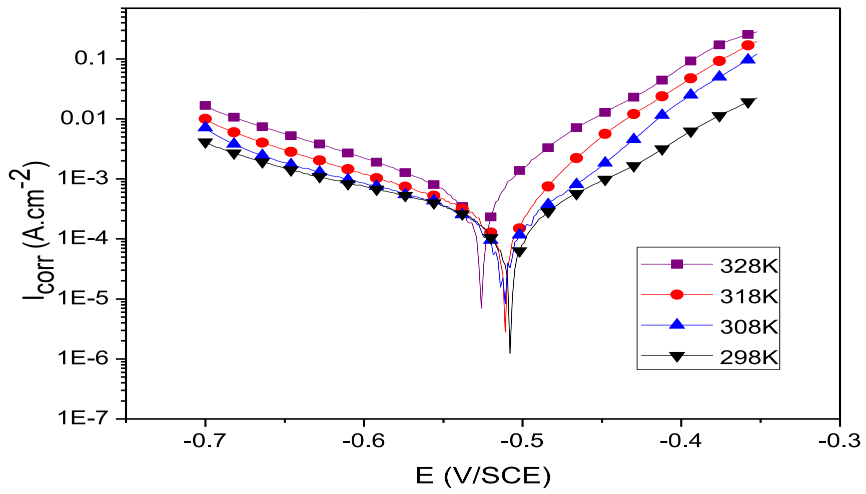

Figure 6. Polarisation curves of C38 steel in 1M HCl.

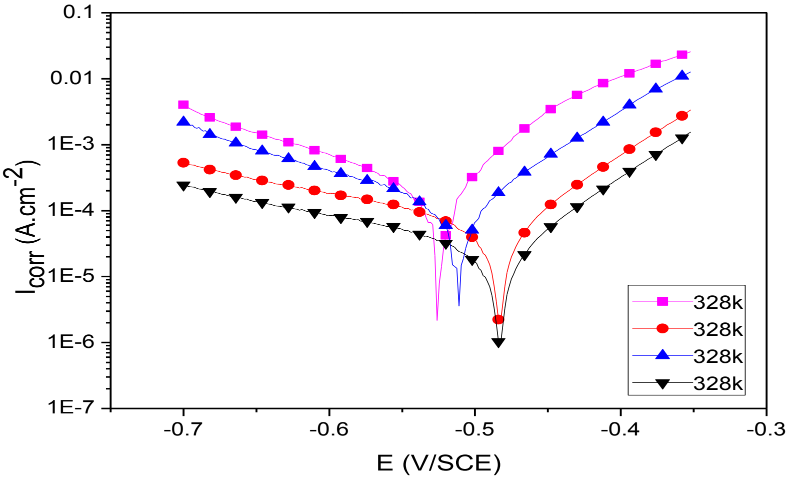

Figure 7. Polarisation curves of C38 steel in 1M HCl in the presence of 10^{-3} M of DNSO at different temperatures.

Table 4. Effect of temperature on the steel corrosion in the absence and presence of DNSO at different concentrations.

Inhibitor	Temperature (K)	E_{corr} (mV/SCE)	I_{corr} (µ /cm^{-2})	bc (mV/dec)	ba (mV/dec)	E (%)
Blank	298	-508	301	-150	69	-
	308	-511	311	-96	52	-
	318	-511	334	-111	47	-
	328	-526	501	-131	50	-
DNSO	298	-445	84	-196	31	72.09
	308	-483	89	-155	48	71.38
	318	-511	111	-142	65	66.77
	328	-525	217	-129	54	56.69

It is clear from fig. 6 and table 4 that the increase of corrosion rate is more pronounced with the rise of temperature for blank solution.

As seen from Fig. 7 and table 4 in the presence of DNSO, I_{corr} is highly reduced. Also, the inhibition efficiency decreases slightly with increasing temperature. This can be explained by the decrease of the strength of adsorption processes at elevated temperature. From this result, we can conclude that DNSO is an excellent inhibitor.

3.2.2 Kinetic parameters

The activation energies of corrosion process in free and inhibited acid were calculated using Arrhenius equation:

$$I_{corr} = A\exp(-\frac{E_a}{R.T}) \qquad (6)$$

where A is Arrhenius factor, Ea is the apparent activation corrosion energy, R is the perfect gas constant and T the absolute temperature.

Plotting (log Icorr) versus 1/T gives straight lines as revealed from Fig.8

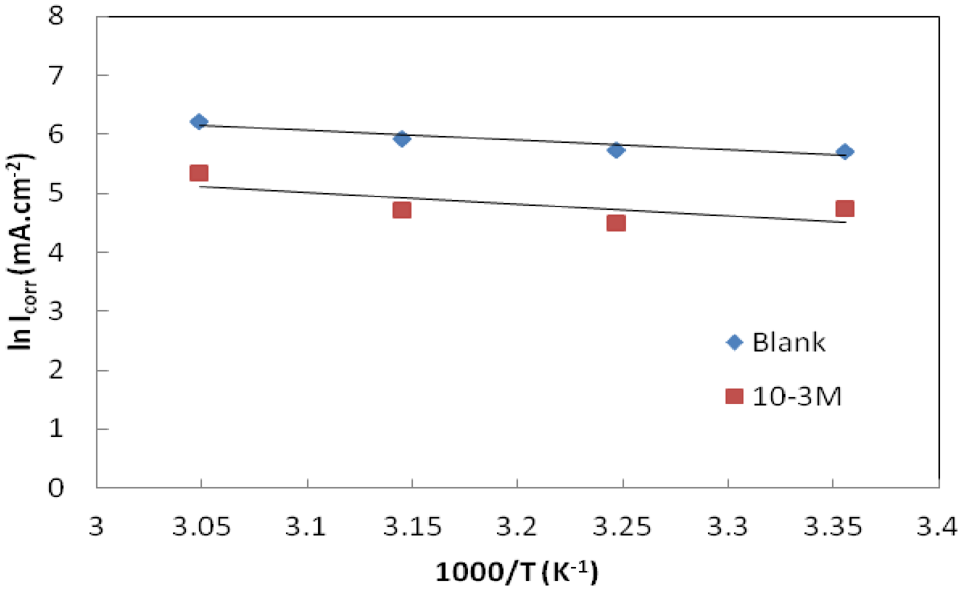

Figure 8. Arrhenius plots of steel in 1 M HCl with and without 10^{-3}M of DNSO

The activation energy values obtained are 16 and 13 kJ/mol for 10^{-3}M of DNSO and free acid, respectively. It's observed that E_a increases in the presence of DNSO that indicates the good performance of this inhibitor at higher temperatures. This increase of activation energy is generally interpreted by an electrostatic adsorption process of inhibitor on the steel surface [40, 41].

Kinetic parameters, such as enthalpy and entropy of corrosion process, may be evaluated from the effect of temperature. An alternative formulation of Arrhenius equation is (6) [42]:

$$I_{corr} = \frac{RT}{Nh}.\exp(\frac{\Delta S^*}{R}).\exp(-\frac{\Delta H^*}{RT}) \qquad (7)$$

Where N is the Avogadro's number, h the Plank's constant, R is the perfect gas constant, ΔS* and ΔH*the entropy and enthalpy of activation, respectively.

Fig. 9 shows a plot of ln(W/T) against 1/T for DNSO. Straight lines are obtained with a slope of (-ΔH*/R) and an intercept of (ln R/Nh + ΔS*/R) from which the values of ΔH*and ΔS* are calculated respectively (Table 5).

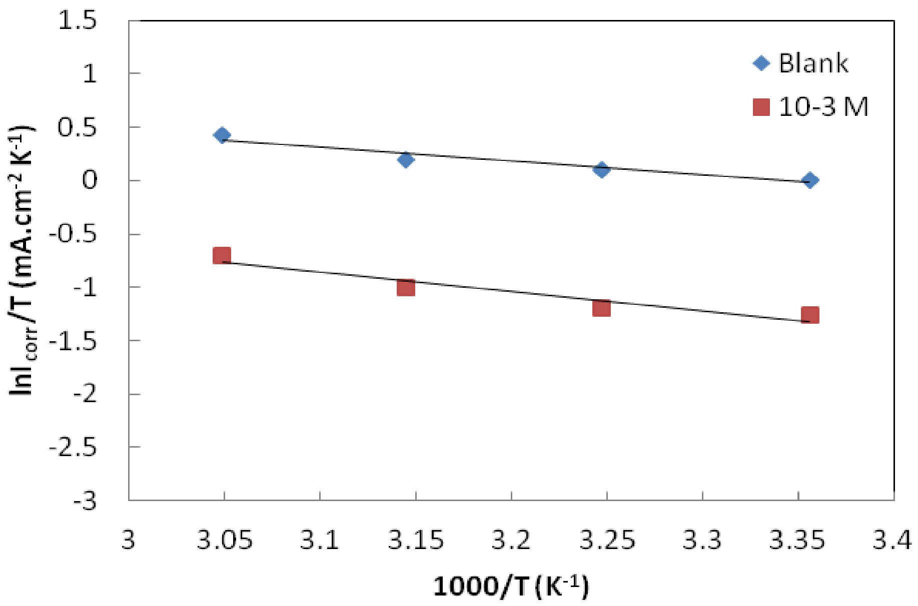

Figure 9. Relation between ln(W_{corr}/T) and 1000/T in acid at different temperatures.

The value of free energy ΔG* is deduced from the formula:

$$\Delta G^* = \Delta H^* - T\Delta S^* \qquad (8)$$

Table 5. The values of activation parameters ΔH^*, ΔS*and ΔG**** for mild steel in 1M HCl in the absence and the presence of 10^{-3} M of DNSO at 298K.

Inhibitor	Conc (M)	ΔH* (kJ/mol)	ΔS* (J/mol^{-1}K^{-1})	ΔG* (kJ/mol)
Blank	0	10.81	- 107.74	42.92
DNSO	10^{-3}	15.29	- 79.29	38.92

The positive signs of ΔH* reflecting the endothermic nature of the steel dissolution process. It is obviously that the activation energy strongly increases in the presence of the inhibitor. Some authors [43- 45] have attributed this result to the inhibitor species being physically adsorbed on the metal surface.

The negative value of entropy ΔS* in the presence of inhibitor imply that the activated complex in the rate determining step represents an association rather than a dissociation step, meaning that an increase in disordering takes place on going from reactants to the activated complex [46].

The ΔG* value for inhibited systems were more positive than that for the uninhibited systems revealing that in presence of inhibitor , the activated corrosion complex becomes less stable as compared to its absence.

3.3. Adsorption isotherm

Additional information about the properties of the tested compounds may be provided from the kind of adsorption isotherm. Several adsorption isotherms were tested and the Langmuir adsorption isotherm was found to provide best description of the adsorption behaviour of the investigated inhibitor. The Langmuir isotherm is given by the equation [47]:

$$\frac{C}{\theta} = \frac{1}{K} + C \qquad (9)$$

$$K = \frac{1}{55.5}\exp\left(-\frac{\Delta G_{ads}}{RT}\right) \qquad (10)$$

Where C is the inhibitor concentration, θ the fraction of the surface covered determined by E/100, k the equilibrium constant, ΔG_{ads} is the standard free energy of adsorption reaction, R is the universal gas constant, T is the thermodynamic temperature and the value of 55.5 is the concentration of water in the solution in mol/L.

Fig. 10 shows the dependence of the ratio C/ θ as function of C.

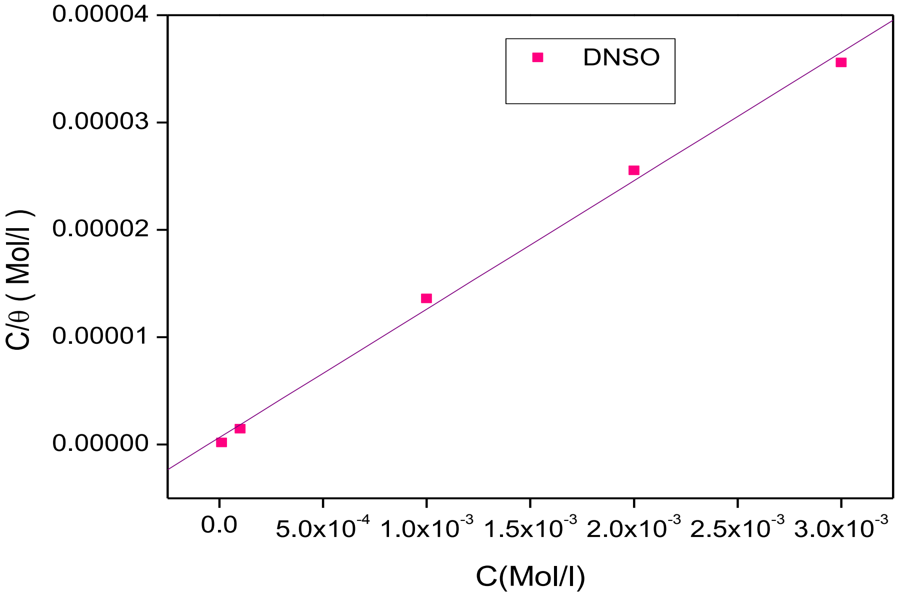

Figure 10. Plots of Langmuir adsorption isotherm of DNSO at 10^{-3}M on the steel surface at 298K.

The value of ΔG_{ads} = -45.2 kJ mol^{-1} is too negative indicating that DNSO is strongly adsorbed on the steel surface [48, 49] and ensuring the spontaneity of the adsorption process. This kind of isotherm is generally regarded as chemisorption [50-52]. The mixed type of inhibitory action revealed that anodic branche is favored by the formation of DNSO-iron ion complex as shown in [53].

4. CONCLUSIONS

The following results can be drawn from this study:

- 2-(ethylthio)-1,4,5-triphenyl-1H-imidazole(DNSO) acts as an excellent mixed inhibitor without modifying the hydrogen reduction mechanism.
- The inhibition efficiency increases with increased DNSO concentration to attain a maximum value of 90.6% at 3.10^{-3}.
- The data obtained from the three different methods: potentiodynamic polarisation, EIS and weight loss, are in good agreements.
- The inhibition efficiency of DNSO decreases with the rise of temperature.
- DNSO studied was adsorbed on the steel surface according to the Langmuir isotherm model.

ACKNOWLEDGEMENTS
Prof S. S. Al-Deyab and Prof B. Hammouti extend their appreciation to the Deanship of Scientific Research at King Saud University for funding the work through the research group project.

References

1. N. O. Eddy, E. E. Ebenso, *Afri. J. Pure Appl. Chem*. 2 (2008) 46.
2. N.O. Eddy, S.A. Odoemelam, *Mat. Sci. India*. 4 (2008) 9.
3. K. Bekkouch, A. Aouniti, B. Hammouti, S.Kertit, *J. Chim. Phys*. 96 (1999) 838.
4. W.A. Badawy, K.M. Ismail, A.M. Fathi, *Electrochim. Acta*. 51 (2006) 4182.
5. D. Bouzidi, S. Kertit, B. Hammouti, M. Brighli, *J. Electrochem. Soc. India*. 46 (1997) 23.
6. S.Kertit, B. Hammouti, M. Taleb, M. Brighli, *Bull. Electrochem*. 13 (1997) 241.
7. B. Hammouti, A. Melhaoui, S. Kertit, *Bull. Electrochem*. 13 (1997) 97.
8. M. Bouklah, N. Benchat, B. Hammouti, A. Aouniti, S. Kertit, *Mater. Lett*. 60 (2006) 1901.
9. D.-Q. Zhang, L.-X. Gao, G.-D. Zhou, *Appl. Surf. Sci*. 252 (2006) 4975.
10. M.T. Saeed, Anti-Corros. *Met. Mater*. 51 (2004) 389.
11. L.G. Qiu, A.J. Xie, Y.H. Shen, *Corros. Sci*. 47 (2005) 273.
12. S. Muralidharan, M.A. Quaraishi, S.V.K. Iyer, *Corros. Sci*. 37 (1995) 1739.
13. B. Hammouti, A. Aouniti, M. Taleb, M. Brighli, S. Kertit, *Corrosion*. 51 (1995) 411.
14. M. Zerfaoui, H. Oudda, B. Hammouti, M. Benkaddour, S. kertit, M. Zertoubi, M. Azzi, M. Taleb, *Revue de Métall*. 99 (2002) 1105.
15. D. Bouzidi, S. Kertit, B. Hammouti, M. Brighli, *J. Electrochem. Soc. India*. 46 (1997) 23.
16. R. Salghi, B. Hammouti, A. Aouniti, M. Berrabah, S. Kertit, *J. Electrochem. Soc. India*. 49 (2000) 40.
17. H. Ashassi-Sorkhabi, Z. Ghasemi, D. Seifzadeh, *Appl. Surf. Sci*. 249 (2005) 408.
18. F. Touhami, B. Hammouti, A. Aouniti, S. Kertit, *Ann. Chim. Sci. Mat*. 24 (1999) 581.
19. A. El-Ouafi, B. Hammouti, H. Oudda, S. Kertit, R. Touzani, A. Ramdani, *Anti-Corros. Met. Mater*. 49 (2002) 199.
20. J. Bartley, N. Huynh, S.E. Bottle, H. Flitt, T. Notoya, D.P. Schweinsberg, *Corros. Sci*. 45 (2003) 81.
21. N. Huynh, S.E. Bottle, T. Notoya, A. Trueman, B. Hinton, D.P. Schweinsberg, *Corros. Sci*. 44 (2002) 1257.
22. R. Salghi, L. Bazzi, B. Hammouti, E. Zine, S. Kertit, S. El Issami, E. Ait Eddi, *Bull. Electrochem*. 17 (2001) 429.

23. A. Aouniti, B. Hammouti, M. Brighli, S. Kertit, F. Berhili, S. El-Kadiri, A. Ramdani, *J. Chim. Phys*. 93 (1996) 1261.
24. A. Yahyi, A. Aouniti, B. Hammouti, A. Ramdani, S. Kertit, *Trans. SAEST* . 39 (2004) 5.
25. M. Bouklah, A. Attayibat, B. Hammouti, A. Ramdani, S. Radi, M. Benkaddour, *Appl. Surf. Sci*. 240 (2005) 341.
26. A. Chetouani, K. Medjahed, K.E. Sid-Lakhdar, B. Hammouti, M. Benkaddour, A. Mansri, *Corros. Sci*. 46 (2004) 2421.
27. S.A. Abd El Maksoud, *J. Electroanal. Chem*. 565 (2004) 321.
28. M. El Azhar, M. Traisnel, B. Mernari, L. Gengembre, F. Bentiss, M. Lagreneé, *Appl. Surf. Sci*. 185 (2002) 197.
29. G. Tarrago, A. Ramdani, J. Elguero, M. Espada, *J. Heterocycl. Chem*. 17 (1980) 137.
30. A. Ramdani, G. Tarrago, *Tetrahedron*. 37 (1981) 987
31. A. Y. El-Etre, *Mat. Chem. Phys*. 108 (2008) 278.
32. S. Kertit, B. Hammouti, Appl. Surf. Sci. 93, 59 (1996)
33. N. Lahhit, A. Bouyanzer, J. M. Desjobert, B. Hammouti, R. Salghi, J. Costa, C. Jama, F. Bentiss, L. Majidi. Portugaliae Electrochimica Acta. 29(2), 127 (2011).
34. O. Benali, L. Larabi, S. M. Mekelleche, Y. Harek, *J. Mater. Sci*. 41 (2006) 7064.
35. O. Benali, L. Larabi, Y. Harek, *J. Appl. Electrochem*. 39 (2009) 769.
36. S. Merah, L. Larabi, O. Benali, Y. Harek, *Pig. Res. Tech*. 37 (5) (2008) 291.
37. H. Ma, S. Chen, B. Yin, S. Zhao, X. Liu, *Corros. Sci*. 45 (2003) 867.
38. E. McCafferty, *Corros. Sci.* 39 (1997) 243.
39. M.S. Morad, *Corros. Sci*. 42 (2000) 1313.
40. A. Popova, E. Sokolova, S.Raicheva, M.Christov, *Corros. Sci*. 45 (2003) 33.
41. T. Szauer, A. Branbt, *Electrochim. Acta*. 22 (1981) 1209.
42. S.S. Abd-El-Rehim, S.A.M. Refaey, F. Taha, M.B. Saleh, R.A. Ahmed, *J. Appl. Electrochem*. 31 (2001) 429.
43. Z. Faska, A. Bellioua, M. Bouklah, L. Majidi, R. Fihi, A. Bouyanzer, B. Hammouti, *Monatshefte für Chemie*. 139 (2008) 1417.
44. A. Bouyanzer, B. Hammouti, *Pigm. Resin & Techn*. 33 (2004) 287.
45. 45.Y. Abboud, A. Abourriche,T. Ainane, M Charrouf, A. Bennamara, O Tanane, B Hammouti, *Chem. Eng. Commun.* 196 (2009) 788.
46. ASTM G1-72, Metal Corrosion, Erosion andWear, Annual Book of ASTM Standards (West Conshohocken, PA: ASTM, (1987), pp. 85-89.
47. F. Mansfeld, M.W. Kending, S. Tsai, *Corrosion*. 37 (1982) 301.
48. J.D. Talati, D.K. Gandhi, Corros. Sci. 23 (1983) 1315.
49. G.K. Gomma, M.H. Wahadan, *Indian J. Chem. Technol*. 2 (1995) 107.
50. I. El Ouali, B. Hammouti, A. Aouniti, Y. Ramli, M. Azougagh, E.M. Essassi, M. Bouachrine, *J. Mater. Environ. Sci.* 1 (2010) 1.
51. M. Dahmani, A. Et-Touhami, S.S. Al-Deyab , B. Hammouti, A. Bouyanzer, *Int. J. Electrochem. Sci*., 5 (2010) 1060.
52. A. Zarrouk, H. Zarrok, R. Salghi, B. Hammouti, F. Bentiss, R. Touir, M. Bouachrine, *J. Mater. Environ. Sci.* 4 (2013) 177
53. Hui-Miao Zhang, Wen-Fu Fu, Shao-Ming Chi, Jun Wang, *J. Luminescence*, 129 (2009) 589.